# Integral Equation Modeling of Cylindrically Periodic Scatterers in the Interior of a Cylindrical Waveguide

Hristos T. Anastassiu, *Member, IEEE,* John L. Volakis, *Fellow, IEEE,* and Dejan S. Filipovic

***Abstract*— We examine the scattering from cylindrically periodic engine-like structures using integral-equation methods. The periodic scatterer is enclosed in a cylindrical waveguide, and the primary goal of this paper is to show that this type of geometry affords substantial computational reductions by exploiting the periodicity of the blade structure and characteristics of the modal scattering matrix of the engine-like termination. Also, as a result of the periodic waveguide termination, a limited number of modes are excited by a given incoming mode, and this is exploited for a further reduction of the storage requirements of the modal scattering matrix.**

***Index Terms*— Cylindrically periodic, discrete body of revolution, method of moments, periodic, scattering.**

## I. Introduction

THE problem of electromagnetic scattering from jet-engine inlets (see Fig. 1) has been investigated in a number of recent papers [1]–[8] via different approaches. Rigorous modal methods [3], [4] are applicable only for simplified engine models since the geometry of a realistic engine termination is not canonical [3]. Also, standard numerical techniques, such as the moment of methods (MoM) or the finite-element method (FEM) cannot handle the entire structure due to its large electrical size. Further, high-frequency techniques such as the shooting and bouncing ray method [6], are not applicable due to the engine's complexity.

For an efficient solution of the problem, it has been found that a decomposition of the computational domain into numerical and high-frequency regions is the most appropriate approach. As shown in Fig. 2, the region surrounding the complex engine termination is modeled numerically, whereas ray or modal methods are used to propagate the field through the duct. In this manner, a significant amount of memory is saved by not discretizing the duct region. One way to couple the two computational regions is through the modal scattering matrix, and this approach is discussed in [1]. However, even with this decomposition, a direct application of numerical methods such as the FDTD [7] and FEM [1] leads to intractable problems when dealing with realistic jet-engine sizes spanning 30 wavelengths in diameter (at 10 GHz). Multispectral characterization requiring radar cross section (RCS) computation at many frequencies introduce additional central processing unit (CPU) time problems.

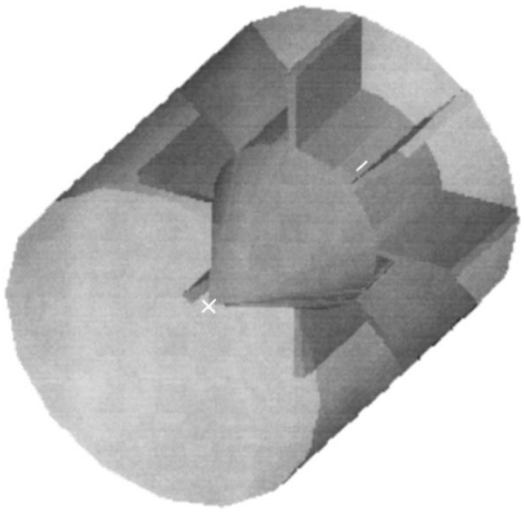

Fig. 1. Simplified model of a jet engine.

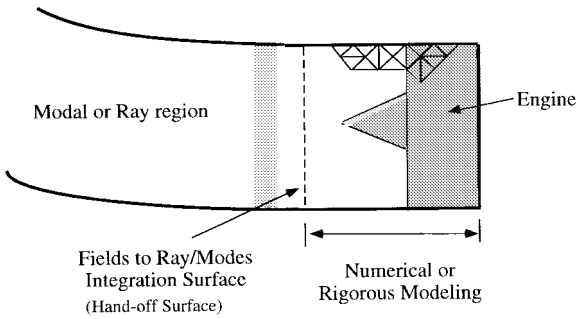


Fig. 2. Illustration of the computational decomposition.

To reduce the CPU time and storage requirements down to manageable levels, we exploit the inherent blade periodicity of the jet engine to show that the computational domain can be reduced down to a single blade or engine "slice." This discrete body of revolution (DBOR) approach reduces the number of unknowns and storage requirements by a factor equal to the number of blades. However, it has so far been implemented only in the context of differential-equation methods [2]. In this paper, we apply the DBOR concept in the context of integral-equation methods for modeling the complex jet-engine configurations. By considering mode-by-mode excitation [1],

Manuscript received October 24, 1996; revised October 30, 1997.

The authors are with the Radiation Laboratory, Department of Electrical Engineering and Computer Science, University of Michigan, Ann Arbor, MI 48109-2122 USA.

Publisher Item Identifier S 0018-9480(98)08003-X.

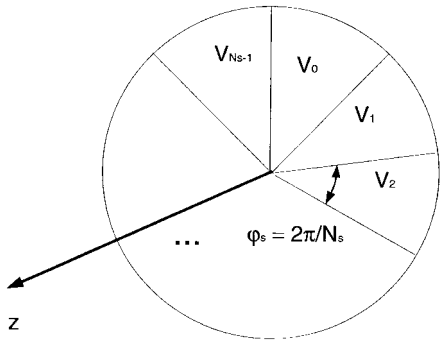


Fig. 3. Symmetry in a DBOR body.

[2], it is shown that the analysis over the entire engine can be reduced down to a surface integral equation over a single blade or periodic sector of the engine. It is further demonstrated that the resulting modal scattering matrix is sparse, leading to additional storage and CPU time reductions.

Further computational reductions can be achieved by incorporating fast integral-equation algorithms such as the adaptive integral method (AIM) [9]. The latter redistributes the currents on the blade onto a canonical grid such that the scattered field due to the fictitious sources on the nodes of the grid remain the same as that of the original sources up to a certain order. Combining blade periodicity and the AIM concept results in drastic complexity reductions.

The DBOR procedure (which takes advantage of blade periodicity) leads to a compact integral equation whose domain is confined over the single engine blade. Initially, we consider perfectly conducting (PEC) scatterers, but the last section of this paper gives an extension of the method to periodic angular sectors containing nonmetallic, possibly lossy, materials. Three appendixes are included, which provide certain mathematical details omitted from the main text, in reference to the dyadic Green's function for cylindrical waveguides and explicit expressions of the elements of the pertinent MoM impedance matrix.

## II. Setup for Perfectly Conducting Scatterers

Consider the PEC scatterer residing inside a cylindrical metallic waveguide and occupying the volume $V$, as shown in Fig. 1. This structure is used to terminate a cylindrical waveguide and consists of $N_s$ periodic sectors or "slices." The slices are identical and rotated around the center axis with respect to each other by integer multiples of the angular period

$$\phi_s = \frac{2\pi}{N_s} \tag{1}$$

where $\phi_s$ is the angular opening of each slice (see Fig. 3). We will refer to this termination as a DBOR since the geometry can be generated by revolving the basic slice occupying the volume $V_0$ a discrete multiple of azimuth angles $\phi_s$. Due to this inherent periodicity, the vector $\boldsymbol{r}$ of a point in the $m_s$th periodic slice occupying the volume $V_{m_s}$ can be written as

$$\boldsymbol{r} = \overline{\overline{\boldsymbol{R}}}^{m_s} \cdot \boldsymbol{r}_0 \quad \boldsymbol{r}_0 \in V_0 \tag{2}$$

where the superscript $m_s$ denotes the power of the dyadic $\overline{\overline{\boldsymbol{R}}}$. The latter is the rotation dyadic, defined in Cartesian coordinates by the matrix

$$[\boldsymbol{R}] = \begin{pmatrix} \cos\phi_s & -\sin\phi_s & 0 \\ \sin\phi_s & \cos\phi_s & 0 \\ 0 & 0 & 1 \end{pmatrix}. \tag{3}$$

It can be readily shown that

$$\overline{\overline{\boldsymbol{R}}}^{-1} = \overline{\overline{\boldsymbol{R}}}^{T} \tag{4}$$

$$\overline{\overline{\boldsymbol{R}}}^{m_s}(\phi_s) = \overline{\overline{\boldsymbol{R}}}(m_s\phi_s). \tag{5}$$

These equations present important properties to be explored later in this analysis.

For the problem of scattering, an incident field $\boldsymbol{E}^i$ is assumed to impinge upon the periodic structure, where $\boldsymbol{E}^i$ is a sum of cylindrical waveguide modes. This excitation induces the surface current $\boldsymbol{J}$ giving rise to the scattered field [10]

$$\boldsymbol{E}^s(\boldsymbol{r}) = -jkZ \int_\Sigma \overline{\overline{\boldsymbol{G}}}(\boldsymbol{r}, \boldsymbol{r}') \cdot \boldsymbol{J}(\boldsymbol{r}')\, d^2S' \tag{6}$$

where $k = \omega\sqrt{\mu\epsilon}$, $Z = \sqrt{\mu/\epsilon}$ ($\mu$ is the permeability, and $\epsilon$ is the permittivity), $\Sigma$ is the outer surface of the scatterer, and $\overline{\overline{\boldsymbol{G}}}$ is the dyadic Green's function for the Helmholtz equation inside a cylinder (electric type of the first kind) stated in Appendix A. An integral equation for $\boldsymbol{J}$ can be derived by invoking the boundary condition satisfied on $\Sigma$, namely,

$$(\boldsymbol{E}^s + \boldsymbol{E}^i) \cdot \boldsymbol{t} = 0 \tag{7}$$

where $\boldsymbol{t}$ is the tangential unit vector on $\Sigma$, demanding that the tangential electric field vanishes on the surface of the periodic scatterer.

A numerical solution for $\boldsymbol{J}$ can be obtained by casting (7) into a discrete system of equations. To do so, we first approximate the surface current $\boldsymbol{J}$ by the expansion

$$\boldsymbol{J}(\boldsymbol{r}') = \sum_q I_q \boldsymbol{f}_q(\boldsymbol{r}') \tag{8}$$

where $\boldsymbol{f}_q(\boldsymbol{r}')$ are the chosen basis functions and $I_q$ are coefficients to be determined. A standard set of linear basis functions are those given by Rao *et al.* [11], which are defined as

$$\boldsymbol{f}_q(\boldsymbol{r}) = \begin{cases} +\dfrac{l_q}{2A_q^+}\boldsymbol{\rho}_q^+, & \text{if } \boldsymbol{r} \in T_q^+ \\ -\dfrac{l_q}{2A_q^-}\boldsymbol{\rho}_q^-, & \text{if } \boldsymbol{r} \in T_q^- \\ \boldsymbol{0}, & \text{otherwise} \end{cases} \tag{9}$$

where $A_q^\pm$ denote the area of the two triangles forming the dihedral patch, as illustrated in Fig. 4. The basis functions represent the current flowing through the $q$th edge from one triangle to the other, where $\boldsymbol{\rho}_q^\pm$ is measured from the vertices opposite to the $q$th edge. A useful property of the basis functions is

$$\boldsymbol{f}_q\left(\overline{\overline{\boldsymbol{R}}}^{m_s} \cdot \boldsymbol{r}\right) = \overline{\overline{\boldsymbol{R}}}^{m_s} \cdot \boldsymbol{f}_q(\boldsymbol{r}) \tag{10}$$

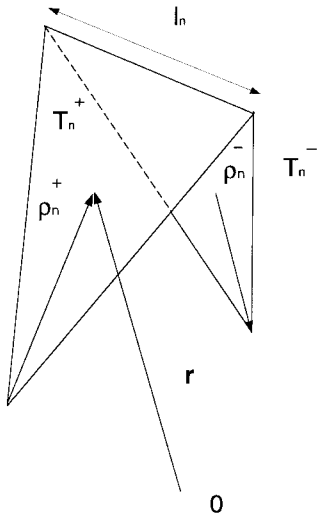


Fig. 4. The Rao–Wilton–Glisson (RWG) linear-surface basis functions.

and this is a consequence of linearity. Substituting (8) into (7), upon Galerkin's testing, we obtain the linear system

$$[\boldsymbol{A}]\{\boldsymbol{I}\} = \{\boldsymbol{V}\} \tag{11}$$

where

$$V_p = \int_{\Sigma} \boldsymbol{E}^i(\boldsymbol{r}) \cdot \boldsymbol{f}_p(\boldsymbol{r})\, d^2S \tag{12}$$

are the elements of the excitation vector $\{\boldsymbol{V}\}$, and $\{\boldsymbol{I}\}$ is the column of unknown current coefficients $I_q$. As usual, $[\boldsymbol{A}]$ is the impedance matrix whose entries are given by

$$A_{pq} = jkZ \int_{\Sigma}\int_{\Sigma} \boldsymbol{f}_p(\boldsymbol{r}) \cdot \overline{\overline{\boldsymbol{G}}}(\boldsymbol{r},\boldsymbol{r}') \cdot \boldsymbol{f}_q(\boldsymbol{r}')\, d^2S\, d^2S'. \tag{13}$$

Note that (11) involves the currents over the *whole* scatterer (see Fig. 1) covering the entire angular domain $0 \leq \phi < 2\pi$. Thus, for large diameter terminations, the size of the impedance matrix quickly becomes unmanageable. In Section III, it will be shown that the scattering from the slices can be isolated from each other, yielding an equivalent system much smaller than (11).

## III. Decoupling of the Linear System of Equations

To exploit the periodicity of the geometry, we proceed to establish a relationship between the currents among the identical slices. Assuming that each periodic slice is identically discretized into $Q$ patches, the current expansion (8) can be rewritten as

$$\boldsymbol{J}(\boldsymbol{r}') = \sum_{m_s=0}^{N_s-1} \sum_{q=1}^{Q} I_q^{(m_s)} \boldsymbol{f}_q\Big(\overline{\overline{\boldsymbol{R}}}^{m_s} \cdot \boldsymbol{r}_0'\Big), \qquad \boldsymbol{r}_0' \in V_0. \tag{14}$$

This is an expression of the total current in terms of local currents on the individual slices with index $m_s$. To facilitate further manipulation, we define the current column vector $\{\boldsymbol{J}\}^{(m_s)}$ of the $m_s$th slice by

$$\{\boldsymbol{J}\}^{(m_s)} \equiv \Big[I_1^{(m_s)}, I_2^{(m_s)}, \cdots, I_Q^{(m_s)}\Big]^T. \tag{15}$$

Using these notations along with identities (4) and (5), (10) can be more explicitly rewritten as

$$\begin{aligned}
&[\boldsymbol{A}]^{(00)}\{\boldsymbol{J}\}^{(0)} + [\boldsymbol{A}]^{(01)}\{\boldsymbol{J}\}^{(1)} + \cdots + [\boldsymbol{A}]^{(0,N_s-1)}\{\boldsymbol{J}\}^{(N_s-1)} \\
&\quad = \{\boldsymbol{b}\}^{(0)} \\
&[\boldsymbol{A}]^{(10)}\{\boldsymbol{J}\}^{(0)} + [\boldsymbol{A}]^{(11)}\{\boldsymbol{J}\}^{(1)} + \cdots + [\boldsymbol{A}]^{(1,N_s-1)}\{\boldsymbol{J}\}^{(N_s-1)} \\
&\quad = \{\boldsymbol{b}\}^{(1)} \\
&\cdots \\
&[\boldsymbol{A}]^{(N_s-1,0)}\{\boldsymbol{J}\}^{(0)} + \cdots + [\boldsymbol{A}]^{(N_s-1,N_s-1)}\{\boldsymbol{J}\}^{(N_s-1)} \\
&\quad = \{\boldsymbol{b}\}^{(N_s-1)}
\end{aligned} \tag{16}$$

where

$$\begin{aligned}
A_{pq}^{(n_s m_s)} \equiv jkZ \int_{\Sigma_0}\int_{\Sigma_0} &\boldsymbol{f}_p(\boldsymbol{r}) \\
&\cdot \overline{\overline{\boldsymbol{R}}}^{-n_s} \cdot \overline{\overline{\boldsymbol{G}}}\Big(\overline{\overline{\boldsymbol{R}}}^{n_s} \cdot \boldsymbol{r}, \overline{\overline{\boldsymbol{R}}}^{m_s} \cdot \boldsymbol{r}'\Big) \cdot \overline{\overline{\boldsymbol{R}}}^{m_s} \\
&\cdot \boldsymbol{f}_q(\boldsymbol{r}')\, d^2S\, d^2S'
\end{aligned} \tag{17}$$

are the entries of the submatrices $[\boldsymbol{A}]^{(n_s m_s)}$ representing the interactions between the $m_s$th and the $n_s$th slice currents. Also, $\{\boldsymbol{b}\}^{(n_s)}$ is the excitation column vector of the $n_s$th slice, defined by

$$\{\boldsymbol{b}\}^{(n_s)} \equiv \Big[V_1^{(n_s)}, V_2^{(n_s)}, \cdots, V_Q^{(n_s)}\Big]^T \tag{18}$$

where

$$V_p^{(n_s)} = \int_{\Sigma_0} \boldsymbol{E}^i\Big(\overline{\overline{\boldsymbol{R}}}^{n_s} \cdot \boldsymbol{r}\Big) \cdot \overline{\overline{\boldsymbol{R}}}^{n_s} \cdot \boldsymbol{f}_p(\boldsymbol{r})\, d^2S. \tag{19}$$

In (19), $\Sigma_0$ is the *outer* surface of the slice within the volume $V_0$. Clearly, the index $m_s$ indicates the slice where the source point is located, whereas $n_s$ is the index representing the slice containing the observation point. Both indexes run from 0 to $N_s - 1$.

To take advantage of blade periodicity, we proceed to establish a relationship among submatrices $[\boldsymbol{A}]^{(n_s m_s)}$. The principal part of the entries of $[\boldsymbol{A}]^{(n_s m_s)}$ can be written as

$$\begin{aligned}
\tilde{A}_{pq}^{(n_s m_s)} = jkZ \sum_{m=1}^{\infty}\sum_{n=-\infty}^{\infty} &e^{-jn(m_s-n_s)\phi_s} \\
&\cdot \Big\{ C_{nm}^{\mathrm{TE}} \int_{\Sigma_0}\int_{\Sigma_0} \boldsymbol{f}_p(\boldsymbol{r}) \cdot \boldsymbol{M}_{nm}(\boldsymbol{r}; \pm\beta_{nm}^{\mathrm{TE}}) \\
&\quad \cdot \boldsymbol{M}_{-nm}(\boldsymbol{r}'; \mp\beta_{nm}^{\mathrm{TE}}) \cdot \boldsymbol{f}_q(\boldsymbol{r}')\, d^2S\, d^2S' \\
&\quad + C_{nm}^{\mathrm{TM}} \int_{\Sigma_0}\int_{\Sigma_0} \boldsymbol{f}_p(\boldsymbol{r}) \cdot \boldsymbol{N}_{nm}(\boldsymbol{r}; \pm\beta_{nm}^{\mathrm{TM}}) \\
&\quad \cdot \boldsymbol{N}_{-nm}(\boldsymbol{r}'; \mp\beta_{nm}^{\mathrm{TM}}) \cdot \boldsymbol{f}_q(\boldsymbol{r}')\, d^2S\, d^2S' \Big\}
\end{aligned} \tag{20}$$

where we have substituted in the cylindrical waveguide the Green's function given in Appendix B. However, any other pertinent Green's function, including that of free space, could be used. From (20), we readily deduce that $A_{pq}^{(n_s m_s)}$ depends only on the difference $m_s - n_s$ and not on the individual values of $m_s$ and $n_s$. This is expected since physical intuition dictates that any interaction between two given slices should depend on

their relative, and not absolute, location. Hence, we introduce the superscript $\kappa_s = m_s - n_s$ to rewrite the system (16) as

$$\begin{aligned}
&[\boldsymbol{A}]^{(0)}\{\boldsymbol{J}\}^{(0)} + [\boldsymbol{A}]^{(1)}\{\boldsymbol{J}\}^{(1)} + \cdots + [\boldsymbol{A}]^{(N_s-1)}\{\boldsymbol{J}\}^{(N_s-1)} \\
&\quad = \{\boldsymbol{b}\}^{(0)} \\
&[\boldsymbol{A}]^{(-1)}\{\boldsymbol{J}\}^{(0)} + [\boldsymbol{A}]^{(0)}\{\boldsymbol{J}\}^{(1)} + \cdots + [\boldsymbol{A}]^{(N_s-2)}\{\boldsymbol{J}\}^{(N_s-1)} \\
&\quad = \{\boldsymbol{b}\}^{(1)} \\
&\cdots \\
&[\boldsymbol{A}]^{(-N_s+1)}\{\boldsymbol{J}\}^{(0)} + \cdots + [\boldsymbol{A}]^{(0)}\{\boldsymbol{J}\}^{(N_s-1)} \\
&\quad = \{\boldsymbol{b}\}^{(N_s-1)}.
\end{aligned} \tag{21}$$

The lone superscript of the impedance submatrices now indicates the relative location of the interacting slices. Since the waveguide and engine fields are identical modulo $2\pi$, it follows that

$$[\boldsymbol{A}]^{(-\kappa_s)} = [\boldsymbol{A}]^{(N_s-\kappa_s)}. \tag{22}$$

This "modulo $N_s$" property will prove extremely important because of its essential role in decoupling the subsystems comprising the overall system (21).

To proceed further, we assume that the incident field is a single cylindrical waveguide mode of order $n_i$, as described in Appendix A. To permit decoupling of the subsystems comprising (21), it is important that the angular dependence be in the form of an exponential and not trigonometric (i.e., the fields must be proportional to $\exp\{jn_i\phi\}$). The excitation column vectors on the $\kappa$th and $(\kappa+1)$th slices are, hence, related via

$$\{\boldsymbol{b}\}^{(\kappa+1)} = e^{jn_i\phi_s}\{\boldsymbol{b}\}^{(\kappa)} \Rightarrow \{\boldsymbol{b}\}^{(\kappa)} = e^{j\kappa n_i\phi_s}\{\boldsymbol{b}\}^{(0)}, \quad \kappa = 0, \cdots, N_s - 1. \tag{23}$$

We will refer to the block rows of (21) by the superscript of the right-hand side, i.e., we will use the terms "zeroth block row," "first block row," ..., "$(N_s-1)$th block row." Now multiplying the $\kappa$th block row of (21) by $e^{-j\kappa n_i\phi_s}$ for all $\kappa = 1, \cdots, N_s - 1$, and subtracting the zeroth block row from all others yields the equivalent system

$$\begin{aligned}
&[\boldsymbol{A}]^{(0)}\{\boldsymbol{J}\}^{(0)} + [\boldsymbol{A}]^{(1)}\{\boldsymbol{J}\}^{(1)} + \cdots + [\boldsymbol{A}]^{(N_s-1)}\{\boldsymbol{J}\}^{(N_s-1)} \\
&\quad = \{\boldsymbol{b}\}^{(0)} \\
&[\boldsymbol{A}]^{(0)}(\{\boldsymbol{J}\}^{(1)}e^{-jn_i\phi_s} - \{\boldsymbol{J}\}^{(0)}) \\
&\qquad + [\boldsymbol{A}]^{(1)}(\{\boldsymbol{J}\}^{(2)}e^{-jn_i\phi_s} - \{\boldsymbol{J}\}^{(1)}) \\
&\qquad + \cdots + [\boldsymbol{A}]^{(N_s-1)}(\{\boldsymbol{J}\}^{(0)}e^{-jn_i\phi_s} - \{\boldsymbol{J}\}^{(N_s-1)}) \\
&\quad = \{\boldsymbol{0}\} \\
&\cdots \\
&[\boldsymbol{A}]^{(0)}(\{\boldsymbol{J}\}^{(N_s-1)}e^{-j(N_s-1)n_i\phi_s} - \{\boldsymbol{J}\}^{(0)}) \\
&\qquad + [\boldsymbol{A}]^{(1)}(\{\boldsymbol{J}\}^{(0)}e^{-j(N_s-1)n_i\phi_s} - \{\boldsymbol{J}\}^{(1)}) \\
&\qquad + \cdots + [\boldsymbol{A}]^{(N_s-1)}(\{\boldsymbol{J}\}^{(N_s-2)}e^{-j(N_s-1)n_i\phi_s} \\
&\qquad - \{\boldsymbol{J}\}^{(N_s-1)}) \\
&\quad = \{\boldsymbol{0}\}
\end{aligned} \tag{24}$$

where we have made use of (22). Apart from the first of these block matrix systems, we can satisfy all other block rows of (24) by setting

$$\begin{aligned}
\{\boldsymbol{J}\}^{(1)} &= e^{jn_i\phi_s}\{\boldsymbol{J}\}^{(0)} \\
\{\boldsymbol{J}\}^{(2)} &= e^{j2n_i\phi_s}\{\boldsymbol{J}\}^{(0)} \\
&\cdots \\
\{\boldsymbol{J}\}^{(N_s-1)} &= e^{j(N_s-1)n_i\phi_s}\{\boldsymbol{J}\}^{(0)}.
\end{aligned} \tag{25}$$

Thus, the top block row of (24) can be written as

$$[\boldsymbol{A}]^{(0)} + \left[[\boldsymbol{A}]^{(1)}e^{jn_i\phi_s} + ... + [\boldsymbol{A}]^{(N_s-1)}e^{j(N_s-1)n_i\phi_s}\right] \cdot\{\boldsymbol{J}\}^{(0)} = \{\boldsymbol{b}\}^{(0)} \tag{26}$$

and since (21) and (24) have the same solution, on the basis of uniqueness, (25) is the only possible choice for relating the periodic sector currents among themselves.

A more compact expression for (26) can be obtained by using the properties of the Green's function. First, we define the left-hand side of (26) as a single matrix $[\boldsymbol{K}]$ as follows:

$$[\boldsymbol{K}] \equiv \left[[\boldsymbol{A}]^{(0)} + [\boldsymbol{A}]^{(1)}e^{jn_i\phi_s} + \cdots + [\boldsymbol{A}]^{(N_s-1)}e^{j(N_s-1)n_i\phi_s}\right]. \tag{27}$$

Next, by using (20) and the geometric sum

$$\begin{aligned}
\Delta_{N_s}(n, n_i) &\equiv \sum_{\kappa_s=0}^{N_s-1} e^{j(n_i-n)\kappa_s\phi_s} \\
&= \begin{cases} N_s, & \text{if } n = n_i + \nu N_s, \quad \nu \in \boldsymbol{Z} \\ 0, & \text{else} \end{cases}
\end{aligned} \tag{28}$$

it follows that the principal part of the matrix entries $K_{pq}$ reduces to

$$\begin{aligned}
\tilde{K}_{pq} = jkZ \sum_{m=1}^{\infty}\sum_{n=-\infty}^{\infty} &\Delta_{N_s}(n, n_i) \\
&\cdot \Big\{ C_{nm}^{\mathrm{TE}} \int_{\Sigma_0}\int_{\Sigma_0} \boldsymbol{f}_p(\boldsymbol{r}) \cdot \boldsymbol{M}_{nm}(\boldsymbol{r}; \pm\beta_{nm}^{\mathrm{TE}}) \\
&\quad \cdot \boldsymbol{M}_{-nm}(\boldsymbol{r}'; \mp\beta_{nm}^{\mathrm{TE}}) \cdot \boldsymbol{f}_q(\boldsymbol{r}')\, d^2S\, d^2S' \\
&\quad \cdot C_{nm}^{\mathrm{TM}} \int_{\Sigma_0}\int_{\Sigma_0} \boldsymbol{f}_p(\boldsymbol{r}) \cdot \boldsymbol{N}_{nm}(\boldsymbol{r}; \pm\beta_{nm}^{\mathrm{TM}}) \\
&\quad \cdot \boldsymbol{N}_{-nm}(\boldsymbol{r}'; \mp\beta_{nm}^{\mathrm{TM}}) \cdot \boldsymbol{f}_q(\boldsymbol{r}')\, d^2S\, d^2S' \Big\}.
\end{aligned} \tag{29}$$

The implication of this result is that for a given order of the incident mode, only a limited set of scattered modes is excited. Namely, only the scattered modes with orders $n$ that satisfy $n = n_i + \nu N_s$, $\nu \in \boldsymbol{Z}$ are reflected back, and this is in agreement with the result given by the FEM analysis of a similar problem [2]. For a body of revolution (BOR), $N_s \to \infty$ and, in this case, (28), implies that $n = n_i$ only, which is consistent with classical BOR theory [12].

The most important consequence of this analysis is that for a given incident mode, it suffices to solve the integral equation

only over a single slice using a modified version of the dyadic Green's function. Indeed, if we define this modified Green's function by the periodicity dyadic

$$\begin{aligned}\overline{\overline{\boldsymbol{I}}}_{n_i}(\boldsymbol{r},\boldsymbol{r}') \equiv & -\frac{1}{k^2}\delta(\boldsymbol{r}-\boldsymbol{r}')\hat{\boldsymbol{z}}\hat{\boldsymbol{z}}' \\ & + \sum_{m=1}^{\infty}\sum_{n=-\infty}^{\infty} \Delta_{N_s}(n,n_i) C_{nm}^{\mathrm{TE}} \\ & \cdot \boldsymbol{M}_{nm}\left(\boldsymbol{r};\pm\beta_{nm}^{\mathrm{TE}}\right)\boldsymbol{M}_{-nm}\left(\boldsymbol{r}';\mp\beta_{nm}^{\mathrm{TE}}\right) \\ & + \sum_{m=1}^{\infty}\sum_{n=-\infty}^{\infty} \Delta_{N_s}(n,n_i) C_{nm}^{\mathrm{TM}} \\ & \cdot \boldsymbol{N}_{nm}(\boldsymbol{r};\pm\beta_{nm}^{\mathrm{TM}})\boldsymbol{N}_{-nm}\left(\boldsymbol{r}';\mp\beta_{nm}^{\mathrm{TM}}\right) \end{aligned} \tag{30}$$

the entries of $[\boldsymbol{K}]$ are given in compact form as

$$K_{pq} = jkZ\int_{\Sigma_0}\int_{\Sigma_0} \boldsymbol{f}_p(\boldsymbol{r})\cdot\overline{\overline{\boldsymbol{I}}}_{n_i}(\boldsymbol{r},\boldsymbol{r}')\cdot\boldsymbol{f}_q(\boldsymbol{r}')\, d^2S\, d^2S'. \tag{31}$$

The currents on the reference slice $\Sigma_0$ are simply the solutions to the system

$$[\boldsymbol{K}]\{\boldsymbol{J}\}^{(0)} = \{\boldsymbol{b}\}^{(0)} \tag{32}$$

and those on the other slices are obtained from (25).

The importance of (32) cannot be exaggerated. Since the problem essentially reduces to modeling only one slice of the scatterer, the number of equations or unknowns is reduced by a factor of $N_s$. For a typical $N_s = 40$, this implies a CPU time and memory reduction each by a factor of 1600. For large scatterers with large periodicity numbers $N_s$, e.g., jet engines, the problem can thus be scaled to a tractable size. Moreover, the limited coupling among the scattered modes results in sparse modal scattering matrices, which are much easier to store and handle. Also, calculations involving the Green's function in (30) can be performed more efficiently since a number of terms corresponding to significant modes of low order are now absent.

Finally, it is important to observe that the above formulation does not demand any restriction on the shape of the periodic slice. Therefore, the shape of the exterior surface of the slices is irrelevant to the integral-equation method and the technique is applicable to arbitrary DBOR's such as realistic jet engines.

## IV. Extension to Dielectric Scatterers

It is straightforward to extend the above analysis to a DBOR which consists of nonmetallic sections. To construct the integral equation, we begin by introducing the scattered field expression

$$\boldsymbol{E}^s(\boldsymbol{r}) = -j\omega\mu\int_V \overline{\overline{\boldsymbol{G}}}(\boldsymbol{r},\boldsymbol{r}')\cdot\boldsymbol{J}_v(\boldsymbol{r}')\, d^3v' \tag{33}$$

where $\boldsymbol{J}_v$ now represents the equivalent-volume current density replacing the dielectric region with permittivity $\epsilon_d(\boldsymbol{r})$ given by

$$\boldsymbol{J}_v(\boldsymbol{r}') = j\omega[\epsilon_d(\boldsymbol{r}')-\epsilon]\boldsymbol{E}(\boldsymbol{r}'). \tag{34}$$

The current density is again expanded into volume basis functions $\boldsymbol{\psi}_q$ via

$$\boldsymbol{J}_v(\boldsymbol{r}') = \sum_q I_q\boldsymbol{\psi}_q(\boldsymbol{r}'). \tag{35}$$

A choice for $\boldsymbol{\psi}_q$ is [13]

$$\boldsymbol{\psi}_q(\boldsymbol{r}) = \sum_{\kappa=1}^{3} P_{q\kappa}(\boldsymbol{r})\hat{\boldsymbol{u}}_\kappa \tag{36}$$

where $\hat{\boldsymbol{u}}_\kappa$, $\kappa = 1,2,3$ denotes unit vectors spanning $\mathcal{R}^3$ and

$$P_{q\kappa}(\boldsymbol{r}) = \begin{cases} 1, & \text{if } \boldsymbol{r}\in\Delta V_q \\ 0, & \text{otherwise.}\end{cases} \tag{37}$$

Using the volume equivalence principle, it can be shown that the integral equation for the current can be written as [13]

$$\boldsymbol{E}^i(\boldsymbol{r}) = j\omega\mu\int_V \overline{\overline{\boldsymbol{G}}}^d(\boldsymbol{r},\boldsymbol{r}')\cdot\boldsymbol{J}_v(\boldsymbol{r}')\, d^3v' \tag{38}$$

where

$$\begin{aligned}\overline{\overline{\boldsymbol{G}}}^d(\boldsymbol{r},\boldsymbol{r}') \equiv & -\frac{\delta(\boldsymbol{r}-\boldsymbol{r}')\hat{\boldsymbol{z}}\hat{\boldsymbol{z}}'}{\omega^2\mu\epsilon_d(\boldsymbol{r}')} - \frac{\delta(\boldsymbol{r}-\boldsymbol{r}')\overline{\overline{\boldsymbol{I}}}}{\omega^2\mu[\epsilon_d(\boldsymbol{r}')-\epsilon]} \\ & + \sum_{m=1}^{\infty}\sum_{n=-\infty}^{\infty} C_{nm}^{\mathrm{TE}}\boldsymbol{M}_{nm}\left(\boldsymbol{r};\pm\beta_{nm}^{\mathrm{TE}}\right) \\ & \cdot \boldsymbol{M}_{-nm}\left(\boldsymbol{r}';\mp\beta_{nm}^{\mathrm{TE}}\right) + \sum_{m=1}^{\infty}\sum_{n=-\infty}^{\infty} \\ & \cdot C_{nm}^{\mathrm{TM}}\boldsymbol{N}_{nm}\left(\boldsymbol{r};\pm\beta_{nm}^{\mathrm{TM}}\right)\boldsymbol{N}_{-nm}\left(\boldsymbol{r}';\mp\beta_{nm}^{\mathrm{TM}}\right) \end{aligned} \tag{39}$$

in which $\overline{\overline{\boldsymbol{I}}}$ is the unit dyadic and $\boldsymbol{M}_{nm}(\boldsymbol{r}), \boldsymbol{N}_{nm}(\boldsymbol{r})$ are defined in Appendix A.

On the basis of a DBOR scatterer

$$\epsilon_d(\overline{\overline{\boldsymbol{R}}}^{m_s}\cdot\boldsymbol{r}) = \epsilon_d(\boldsymbol{r}) \qquad \forall m_s\in\boldsymbol{Z} \tag{40}$$

and by invoking a similar procedure as in the case of metallic scatterers, we can express the entries of the impedance submatrix $[\boldsymbol{A}]^{(n_s m_s)}$ as

$$\begin{aligned}A_{pq}^{(n_s m_s)} = & -\frac{j}{\omega}\delta_{m_s n_s}\int_{V_0}\frac{1}{\epsilon_d(\boldsymbol{r})}\,[\boldsymbol{\psi}_p(\boldsymbol{r})\cdot\hat{\boldsymbol{z}}][\boldsymbol{\psi}_q(\boldsymbol{r})\cdot\hat{\boldsymbol{z}}]\, d^3v \\ & - \frac{j}{\omega}\delta_{m_s n_s}\int_{V_0}\frac{1}{[\epsilon_d(\boldsymbol{r})-\epsilon]}\boldsymbol{\psi}_p(\boldsymbol{r})\cdot\boldsymbol{\psi}_q(\boldsymbol{r})\, d^3v \\ & + j\omega\mu\sum_{m=1}^{\infty}\sum_{n=-\infty}^{\infty} e^{-jn(m_s-n_s)\phi_s} \\ & \cdot\Big\{C_{nm}^{\mathrm{TE}}\int_{V_0}\int_{V_0}\boldsymbol{\psi}_p(\boldsymbol{r})\cdot\boldsymbol{M}_{nm}(\boldsymbol{r};\pm\beta_{nm}^{\mathrm{TE}}) \\ & \cdot\boldsymbol{M}_{-nm}\left(\boldsymbol{r}';\mp\beta_{nm}^{\mathrm{TE}}\right)\cdot\boldsymbol{\psi}_q(\boldsymbol{r}')\, d^3v\, d^3v' \\ & + C_{nm}^{\mathrm{TM}}\int_{V_0}\int_{V_0}\boldsymbol{\psi}_p(\boldsymbol{r})\cdot\boldsymbol{N}_{nm}\left(\boldsymbol{r};\pm\beta_{nm}^{\mathrm{TM}}\right) \\ & \cdot\boldsymbol{N}_{-nm}\left(\boldsymbol{r}';\mp\beta_{nm}^{\mathrm{TM}}\right)\cdot\boldsymbol{\psi}_q(\boldsymbol{r}')\, d^3v\, d^3v'\Big\} \end{aligned} \tag{41}$$

where $\delta_{mn}$ is the Kronecker delta. Also, the entries of the excitation column vector are given by [cf. (19)]

$$V_p^{(n_s)} = \int_{V_0}\boldsymbol{E}^i(\overline{\overline{\boldsymbol{R}}}^{n_s}\cdot\boldsymbol{r})\cdot\overline{\overline{\boldsymbol{R}}}^{n_s}\cdot\boldsymbol{\psi}_p(\boldsymbol{r})\, d^3v. \tag{42}$$

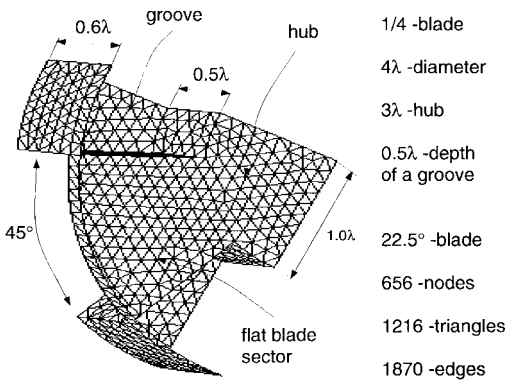


Fig. 5. Mesh and geometry parameters for one-fourth of the engine termination (single slice).

Apart from a slight modification, the expressions for the impedance matrix and excitation vector are nearly identical to those for the PEC DBOR. For reference, the periodicity dyadic in (30) for the dielectric DBOR is

$$\begin{aligned}\overline{\overline{\boldsymbol{I}}}^{d}_{n_i}(\boldsymbol{r},\boldsymbol{r}') \equiv & -\frac{\delta(\boldsymbol{r}-\boldsymbol{r}')\hat{\boldsymbol{z}}\hat{\boldsymbol{z}}'}{\omega^2\mu\epsilon_d(\boldsymbol{r}')} - \frac{\delta(\boldsymbol{r}-\boldsymbol{r}')\overline{\overline{\boldsymbol{I}}}}{\omega^2\mu[\epsilon_d(\boldsymbol{r}')-\epsilon]} \\ & + \sum_{m=1}^{\infty}\sum_{n=-\infty}^{\infty} \Delta_{N_s}(n,n_i) C^{\mathrm{TE}}_{nm} \boldsymbol{M}_{nm}\left(\boldsymbol{r};\pm\beta^{\mathrm{TE}}_{nm}\right) \\ & \cdot \boldsymbol{M}_{-nm}\left(\boldsymbol{r}';\mp\beta^{\mathrm{TE}}_{nm}\right) \\ & + \sum_{m=1}^{\infty}\sum_{n=-\infty}^{\infty} \Delta_{N_s}(n,n_i) C^{\mathrm{TM}}_{nm} \boldsymbol{N}_{nm}\left(\boldsymbol{r};\pm\beta^{\mathrm{TM}}_{nm}\right) \\ & \cdot \boldsymbol{N}_{-nm}\left(\boldsymbol{r}';\mp\beta^{\mathrm{TM}}_{nm}\right) \end{aligned} \tag{43}$$

## V. Validation and Results

As an example, let as consider a four-blade geometry in a cylindrical waveguide, as shown in Fig. 5. For this configuration, the diameter of the cylinder was chosen to be $4\lambda$, and the length of the engine and duct was $3.6\lambda$. The straight blades occupied $90^0$ angular sectors and were facing parallel to the cylinder's base, forming the grooves shortage. Based on the proposed formulation, only a single blade was needed and, in doing so, the memory was reduced from 855 to 53 MB. The CPU time is typically reduced by the same factor of $(N_s)^2$, i.e., the efficiency of the DBOR method is increased along with the number of blades. Scattering patterns ($\phi\phi$ and $\theta\theta$ polarizations) for the geometries shown in Fig. 5 are given in Figs. 6 and 7.

The reference data are based on the mode-matching method [3] and, except for the lower RCS regions (nulls), they are in good agreement with the DBOR MoM data. The differences are attributed to the mode-matching method that typically suffers from mode convergence and field-modeling inaccuracies near the edges of the blades.

## VI. Summary and Conclusions

In this paper, we showed that substantial computational efficiency can be achieved by taking advantage of the periodicity properties of DBOR (e.g., a jet engine) situated in a cylindrical waveguide. Specifically, the following simplifications were

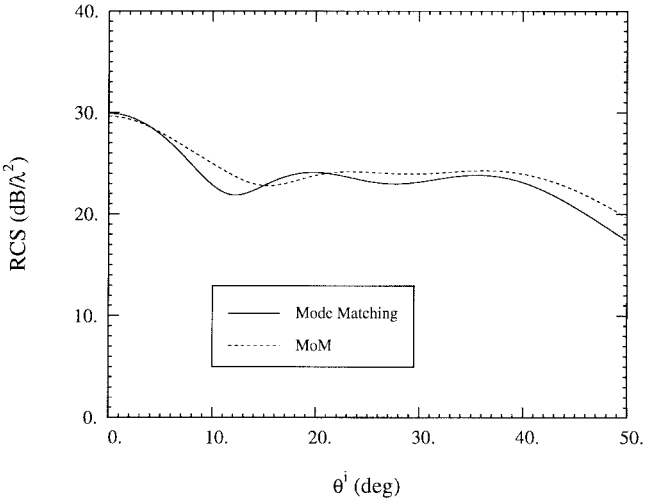


Fig. 6. Backscatter RCS for the four straight blades engine ($\phi$ polarization, $\phi = 0$ cut).

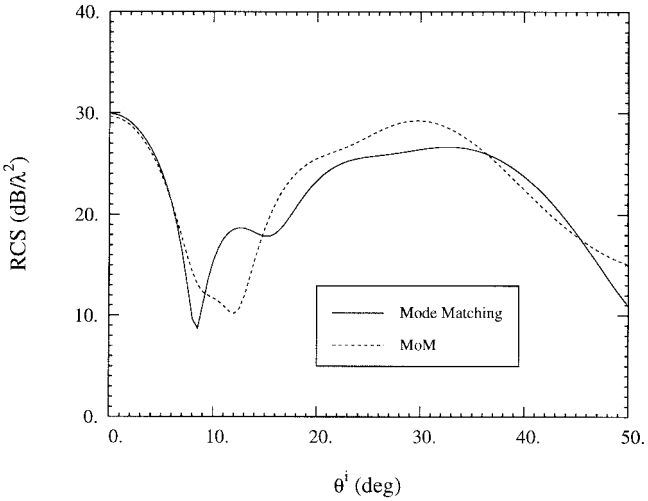


Fig. 7. Backscatter RCS for the four straight blades engine ($\theta$ polarization, $\phi = 0$ cut).

achieved. The modal scattering matrix is very sparse and its nonzero entries can be predicted *a priori*, leading to large storage savings. The computational domain can be reduced down to a single periodic sector of the scatterer (e.g., a single blade for the jet engine). This is done regardless of the geometry of the periodic sector or slice and, as can be realized, the computational savings are dramatic. Specifically, the number of unknowns is reduced by a factor equal to the number of slices $N_s$, with the corresponding computational savings being equal to $(N_s)^2$. The above CPU time simplifications for a DBOR parallel those already known for regular BOR's and, therefore, this analysis can be considered as a generalization of the latter. Similar simplifications can be carried out for partial differential equation (PDE) simulations. However, the incorporation of the DBOR concept in the integral-equation formulation is more attractive for metallic structures because the computational domain is restricted to the scatterer's surface and no cumbersome phase boundary conditions are needed to take advantage of periodicity. Instead, for integral equations,

the only modification is the introduction of the periodic Green's function.

Results for jet-engine configurations with straight blades were given for validation purposes. However, the proposed DBOR method has been equally well applied to realistic jet engines, which involve twisted blades and conical–cylindrical hub sections.

## APPENDIX A
## THE CYLINDRICAL WAVEGUIDE DYADIC GREEN'S FUNCTION

Following [10], we define two sets of cylindrical vector wave functions, namely,

$$\boldsymbol{M}_{nm}(\boldsymbol{r};\beta_{nm}^{\mathrm{TE}}) \equiv \nabla \times \left[J_{|n|}\left(\gamma_{nm}^{\mathrm{TE}}\rho\right)e^{jn\phi}e^{-j\beta_{nm}^{\mathrm{TE}}z}\hat{\boldsymbol{z}}\right] \tag{44}$$

$$\boldsymbol{N}_{nm}(\boldsymbol{r};\beta_{nm}^{\mathrm{TM}}) \equiv \frac{1}{k}\nabla \times \nabla \times \left[J_{|n|}\left(\gamma_{nm}^{\mathrm{TM}}\rho\right)e^{jn\phi}e^{-j\beta_{nm}^{\mathrm{TM}}z}\hat{\boldsymbol{z}}\right]. \tag{45}$$

The functions $\boldsymbol{M}_{nm}$ correspond to TE modes and the functions $\boldsymbol{N}_{nm}$ are associated with TM modes. If the waveguide radius is $a$, then $\gamma_{nm}^{\mathrm{TM,TE}}$ and $\beta_{nm}^{\mathrm{TM,TE}}$ are defined by

$$J_n\left(\gamma_{nm}^{\mathrm{TM}}a\right) = 0 \tag{46}$$

$$J_n'\left(\gamma_{nm}^{\mathrm{TE}}a\right) = 0 \tag{47}$$

$$\left(\gamma_{nm}^{\mathrm{TM,TE}}\right)^2 + \left(\beta_{nm}^{\mathrm{TM,TE}}\right)^2 = k^2. \tag{48}$$

Carrying out the vector operations, $\boldsymbol{M}_{nm}$ and $\boldsymbol{N}_{nm}$ can be written explicitly as

$$\begin{aligned}\boldsymbol{M}_{nm}(\boldsymbol{r};\beta_{nm}^{\mathrm{TE}}) =& \frac{jn}{\rho}J_{|n|}\left(\gamma_{nm}^{\mathrm{TE}}\rho\right)e^{jn\phi}e^{-j\beta_{nm}^{\mathrm{TE}}z}\hat{\boldsymbol{\rho}} \\ &- \gamma_{nm}^{\mathrm{TE}}J_{|n|}'\left(\gamma_{nm}^{\mathrm{TE}}\rho\right)e^{jn\phi}e^{-j\beta_{nm}^{\mathrm{TE}}z}\hat{\boldsymbol{\phi}}\end{aligned} \tag{49}$$

$$\begin{aligned}\boldsymbol{N}_{nm}(\boldsymbol{r};\beta_{nm}^{\mathrm{TM}}) =& -\frac{j\gamma_{nm}^{\mathrm{TM}}\beta_{nm}^{\mathrm{TM}}}{k}J_{|n|}'(\gamma_{nm}^{\mathrm{TM}}\rho)e^{jn\phi}e^{-j\beta_{nm}^{\mathrm{TM}}z}\hat{\boldsymbol{\rho}} \\ &+ \frac{n\beta_{nm}^{\mathrm{TM}}}{k\rho}J_{|n|}\left(\gamma_{nm}^{\mathrm{TM}}\rho\right)e^{jn\phi}e^{-j\beta_{nm}^{\mathrm{TM}}z}\hat{\boldsymbol{\phi}} \\ &+ \frac{(\gamma_{nm}^{\mathrm{TM}})^2}{k}J_{|n|}\left(\gamma_{nm}^{\mathrm{TM}}\rho\right)e^{jn\phi}e^{-j\beta_{nm}^{\mathrm{TM}}z}\hat{\boldsymbol{z}}.\end{aligned} \tag{50}$$

The dyadic Green's function of the electric type satisfying Dirichlet boundary conditions (first kind) is given by

$$\begin{aligned}\overline{\overline{\boldsymbol{G}}}(\boldsymbol{r},\boldsymbol{r}') =& -\frac{1}{k^2}\delta(\boldsymbol{r}-\boldsymbol{r}')\hat{\boldsymbol{z}}\hat{\boldsymbol{z}}' + \sum_{m=1}^{\infty}\sum_{n=-\infty}^{\infty} \\ &\cdot C_{nm}^{\mathrm{TE}}\boldsymbol{M}_{nm}\left(\boldsymbol{r};\pm\beta_{nm}^{\mathrm{TE}}\right)\boldsymbol{M}_{-nm}\left(\boldsymbol{r}';\mp\beta_{nm}^{\mathrm{TE}}\right) \\ &+ \sum_{m=1}^{\infty}\sum_{n=-\infty}^{\infty} C_{nm}^{\mathrm{TM}}\boldsymbol{N}_{nm}\left(\boldsymbol{r};\pm\beta_{nm}^{\mathrm{TM}}\right) \\ &\cdot \boldsymbol{N}_{-nm}\left(\boldsymbol{r}';\mp\beta_{nm}^{\mathrm{TM}}\right)\end{aligned} \tag{51}$$

where the upper sign is used for $z \geq z'$ and the lower sign for $z < z'$. The constants are given by

$$C_{nm}^{\mathrm{TE}} = -j\left\{2\pi\left[\left(\gamma_{nm}^{\mathrm{TE}}a\right)^2 - n^2\right]J_{|n|}^2\left(\gamma_{nm}^{\mathrm{TE}}a\right)\beta_{nm}^{\mathrm{TE}}\right\}^{-1} \tag{52}$$

$$C_{nm}^{\mathrm{TM}} = -j\left\{2\pi\left(\gamma_{nm}^{\mathrm{TM}}a\right)^2\left[J_{|n|}'\left(\gamma_{nm}^{\mathrm{TM}}a\right)\right]^2\beta_{nm}^{\mathrm{TM}}\right\}^{-1}. \tag{53}$$

Notice that exponential, and not trigonometric, dependence on $\phi$ is used.

## APPENDIX B
## ELEMENTS OF THE IMPEDANCE MATRIX FOR PEC SCATTERERS

In the text of this paper, we showed that the impedance matrix entries for PEC terminations are given by

$$\begin{aligned}A_{pq}^{(n_s m_s)} =& jkZ\int_{\Sigma_0}\int_{\Sigma_0}\boldsymbol{f}_p(\boldsymbol{r})\cdot\overline{\overline{\boldsymbol{R}}}^{-n_s}\cdot\overline{\overline{\boldsymbol{G}}}\left(\overline{\overline{\boldsymbol{R}}}^{n_s}\cdot\boldsymbol{r},\overline{\overline{\boldsymbol{R}}}^{m_s}\cdot\boldsymbol{r}'\right) \\ &\cdot\overline{\overline{\boldsymbol{R}}}^{m_s}\cdot\boldsymbol{f}_q(\boldsymbol{r}')\,d^2S\,d^2S'\end{aligned} \tag{54}$$

where $\overline{\overline{\boldsymbol{R}}}$ is the rotation dyadic. To eliminate the rotation dyadics, we can use the properties of $\overline{\overline{\boldsymbol{G}}}$ as defined in Appendix A. First, we express $\boldsymbol{M}_{nm}(\boldsymbol{r})$ as

$$\boldsymbol{M}_{nm}(\boldsymbol{r}) = \sum_{i=1}^{3}M_{nm}^{(i)}(\boldsymbol{r})\hat{\boldsymbol{e}}_i(\boldsymbol{r}) \tag{55}$$

where $\{\hat{\boldsymbol{e}}_1,\hat{\boldsymbol{e}}_2,\hat{\boldsymbol{e}}_3\} = \{\hat{\boldsymbol{\rho}},\hat{\boldsymbol{\phi}},\hat{\boldsymbol{z}}\}$. It then follows that

$$\begin{aligned}\boldsymbol{M}_{nm}\left(\overline{\overline{\boldsymbol{R}}}^{\kappa_s}\cdot\boldsymbol{r}\right) &= \sum_{i=1}^{3}M_{nm}^{(i)}\left(\overline{\overline{\boldsymbol{R}}}^{\kappa_s}\cdot\boldsymbol{r}\right)\hat{\boldsymbol{e}}_i\left(\overline{\overline{\boldsymbol{R}}}^{\kappa_s}\cdot\boldsymbol{r}\right) \\ &= e^{jn\kappa_s\phi_s}\sum_{i=1}^{3}M_{nm}^{(i)}(\boldsymbol{r})\overline{\overline{\boldsymbol{R}}}^{\kappa_s}\cdot\hat{\boldsymbol{e}}_i(\boldsymbol{r}) \\ &= e^{jn\kappa_s\phi_s}\sum_{i=1}^{3}M_{nm}^{(i)}\hat{\boldsymbol{e}}_i(\boldsymbol{r})\cdot\overline{\overline{\boldsymbol{R}}}^{-\kappa_s} \\ &= e^{jn\kappa_s\phi_s}\boldsymbol{M}_{nm}(\boldsymbol{r})\cdot\overline{\overline{\boldsymbol{R}}}^{-\kappa_s}.\end{aligned} \tag{56}$$

Similarly,

$$\boldsymbol{N}_{nm}\left(\overline{\overline{\boldsymbol{R}}}^{\kappa_s}\cdot\boldsymbol{r}\right) = e^{jn\kappa_s\phi_s}\boldsymbol{N}_{nm}(\boldsymbol{r})\cdot\overline{\overline{\boldsymbol{R}}}^{-\kappa_s}. \tag{57}$$

Next, we define the principal part $\tilde{A}_{pq}^{(n_s m_s)}$ of (54) as the integral over the modes only [not including the delta function term in (51)]. By invoking (56) and (57), (54) yields

$$\begin{aligned}\tilde{A}_{pq}^{(n_s m_s)} =& jkZ\sum_{m=1}^{\infty}\sum_{n=-\infty}^{\infty}e^{-jn(m_s-n_s)\phi_s} \\ &\cdot\left\{C_{nm}^{\mathrm{TE}}\int_{\Sigma_0}\int_{\Sigma_0}\boldsymbol{f}_p(\boldsymbol{r})\cdot\boldsymbol{M}_{nm}\left(\boldsymbol{r};\pm\beta_{nm}^{\mathrm{TE}}\right)\right. \\ &\cdot\boldsymbol{M}_{-nm}(\boldsymbol{r}';\mp\beta_{nm}^{\mathrm{TE}})\cdot\boldsymbol{f}_q(\boldsymbol{r}')\,d^2S\,d^2S' \\ &+ C_{nm}^{\mathrm{TM}}\int_{\Sigma_0}\int_{\Sigma_0}\boldsymbol{f}_p(\boldsymbol{r})\cdot\boldsymbol{N}_{nm}\left(\boldsymbol{r};\pm\beta_{nm}^{\mathrm{TM}}\right) \\ &\left.\cdot\boldsymbol{N}_{-nm}\left(\boldsymbol{r}';\mp\beta_{nm}^{\mathrm{TM}}\right)\cdot\boldsymbol{f}_q(\boldsymbol{r}')\,d^2S\,d^2S'\right\}.\end{aligned} \tag{58}$$

## APPENDIX C
## SCATTERED FIELD FROM PEC DBOR'S

It is possible to express the scattered field from a PEC DBOR in a very compact form involving the currents of the reference slice $\Sigma_0$. Given an incident mode of order $n_i$, the scattered field is generally given by (6). Using the properties

of the dyadic Green's function and (14), together with (25), after some algebra similar to Appendix B, we deduce that for a point $\boldsymbol{r}$ away from the scatterer, such that $z > z'$ for any source point $\boldsymbol{r}'$,

$$\boldsymbol{E}^s_{n_i}(\boldsymbol{r}) = -jkZ \sum_{m=1}^{\infty} \sum_{n=-\infty}^{\infty} \Big[ B^{\mathrm{TE}}_{nm,n_i} \boldsymbol{M}_{nm}(\boldsymbol{r}; \beta^{\mathrm{TE}}_{nm}) + B^{\mathrm{TM}}_{nm,n_i} \boldsymbol{N}_{nm}(\boldsymbol{r}; \beta^{\mathrm{TM}}_{nm}) \Big] \tag{59}$$

where

$$B^{\mathrm{TE}}_{nm,n_i} \equiv \Delta_{N_s}(n, n_i) C^{\mathrm{TE}}_{nm} \sum_{q=1}^{Q} I^{(0)}_{q,n_i} \int_{\Sigma_0} \boldsymbol{M}_{-nm}(\boldsymbol{r}'; -\beta^{\mathrm{TE}}_{nm}) \cdot \boldsymbol{f}_q(\boldsymbol{r}')\, d^2S' \tag{60}$$

$$B^{\mathrm{TM}}_{nm,n_i} \equiv \Delta_{N_s}(n, n_i) C^{\mathrm{TM}}_{nm} \sum_{q=1}^{Q} I^{(0)}_{q,n_i} \int_{\Sigma_0} \boldsymbol{N}_{-nm}(\boldsymbol{r}'; -\beta^{\mathrm{TM}}_{nm}) \cdot \boldsymbol{f}_q(\boldsymbol{r}')\, d^2S'. \tag{61}$$

Evidently, (59) yields the scattered field in terms of TE and TM modes, whereas the coefficients of the expansion (i.e., the elements of the modal scattering matrix) are conveniently given by (60) and (61) in terms of the currents $I^{(0)}_{q,n_i}$ on slice $\Sigma_0$ only. A similar expression holds for dielectric scatterers. We again emphasize that due to the term $\Delta_{N_s}(n, n_i)$, only a limited set of scattered modes are returned.

## REFERENCES


[1] D. C. Ross, J. L. Volakis, and H. T. Anastassiu, "Hybrid finite element-modal analysis of jet engine inlet scattering," *IEEE Trans. Antennas Propagat.*, vol. 43, pp. 277–285, Mar. 1995.

[2] ———, "Overlapping modal and geometric symmetries for computing jet engine inlet scattering," *IEEE Trans. Antennas Propagat.*, vol. 43, pp. 1159–1163, Oct. 1995.

[3] H. T. Anastassiu, J. L. Volakis, and D. C. Ross, "The mode matching technique for electromagnetic scattering by cylindrical waveguides with canonical terminations," *J. Electromag. Waves Applicat.*, vol. 9, no. 11/12, pp. 1363–1391, Nov./Dec. 1995.

[4] H. T. Anastassiu, J. L. Volakis, D. C. Ross, and D. Andersh, "Electromagnetic scattering from simple jet engine models", *IEEE Trans. Antennas Propagat.*, vol. 44, pp. 420–421, Mar. 1996.

[5] P. H. Pathak and R. J. Burkholder, "High-frequency EM scattering by open-ended waveguide cavities," *Radio Sci.*, vol. 26, no. 1, pp. 211–218, Jan.–Feb. 1991.

[6] H. Ling, R. C. Chou, and S. W. Lee, "Shooting and bouncing rays: Calculating the RCS of an arbitrarily shaped cavity," *IEEE Trans. Antennas Propagat.*, vol. 37, pp. 194–205, Feb. 1989.

[7] R. Lee and T. T. Chia, "Analysis of electromagnetic scattering from a cavity with a complex termination by means of a hybrid ray FDTD method," *IEEE Trans. Antennas Propagat.*, vol. 41, pp. 1560–1669, Nov. 1993.

[8] J. L. Karty, J. M. Roedder, and S. D. Alspach, "CAVERN: A prediction code for cavity electromagnetic analysis," *IEEE Antennas Propagat. Mag.*, vol. 37, no. 3, pp. 68–72, June 1995.

[9] E. Bleszynski, M. Bleszynski, and T. Jaroszewicz, "AIM: Adaptive integral method for solving large-scale electromagnetics scattering and radiation problems,"*Radio Sci.*, vol. 31, no. 5, pp. 1225–1251, Sept.–Oct. 1996.

[10] C.-T. Tai, *Dyadic Green Functions in Electromagnetic Theory*. Piscataway, NJ: IEEE Press, 1994.

[11] S. M. Rao, D. R. Glisson, and A. W. Wilton "Electromagnetic scattering by surfaces of arbitrary shape," *IEEE Trans. Antennas Propagat.*, vol. 30, pp. 409–418, May 1982.

[12] J. R. Mautz and R. F. Harrington, "Radiation and scattering from bodies of revolution," *Appl. Sci. Res.*, vol. 20, pp. 405–435, June 1969.

[13] J. J. H. Wang, "Analysis of a three-dimensional arbitrary shaped dielectric or biological body inside a rectangular waveguide," *IEEE Trans. Microwave Theory Tech.*, vol. MTT-26, pp. 457–461, July 1978.


**Hristos T. Anastassiu** (S'89–M'91), photograph and biography not available at the time of publication.

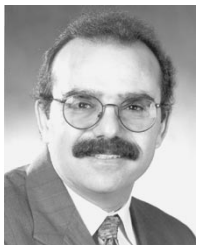

**John L. Volakis** (S'77–A'79–M'82–SM'88–F96) was born in Chios, Greece, on May 13, 1956. He received the B.E. degree (*summa cum laude*) from Youngstown State University, Youngstown, OH, in 1978, and the M.Sc. and Ph.D. degrees from the Ohio State University, Columbus, in 1979 and 1982, respectively.

From 1978 to 1982, he was a Graduate Research Associate at the Ohio State University ElectroScience Laboratory. From 1982 to 1984, he was with Rockwell International, Aircraft Division. Since 1984, he has been with the University of Michigan at Ann Arbor, where he is currently a Professor in the Department of Electrical Engineering and Computer Science (EECS). His primary research deals with the development and application of analytical and numerical techniques to large-scale scattering, printed antennas, and bioelectromagnetics. Along with his students, he developed prototype algorithms and computer codes for modeling antennas, radar scattering and imaging of aircraft structures and microwave circuits. He has published approximately 140 articles in major refereed journal articles, over 140 conference papers, several book chapters on numerical methods, and has co-authored: *Approximate Boundary Conditions in Electromagnetics* (London, U.K.: Inst. Elect. Eng. Press, 1995) and *Finite-Element Method for Electromagnetics* (Piscataway, NJ: IEEE Press, 1998). He was an Associate Editor of *Radio Science* from 1994 to 1997. He is an Associate Editor for the *J. Electromagnetic Waves and Applications*

Dr. Volakis is a member of Sigma Xi, Tau Beta Pi, Phi Kappa Phi, and Commission B of URSI. He is also a member of the AdCom for the IEEE Antennas and Propagation Society. He has served as an Associate Editor of the IEEE TRANSACTIONS ON ANTENNAS AND PROPAGATION (1988–1992), and chaired the 1993 IEEE Antennas and Propagation Society Symposium and Radio Science Meeting. He is currently an associate editor for *IEEE Antennas and Propagation Society Magazine*. In 1998, he received the University of Michigan College of Engineering Research Excellence Award.

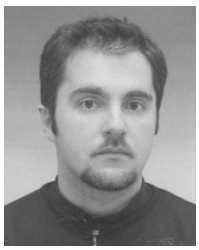

**Dejan S. Filipovic** received the Dipl.Ing. degree in electrical engineering from the University of Nish, Nish, Yugoslavia, in 1994.

Upon graduation, he worked as an Research Assistant at the Faculty of Electronic Engineering, University of Nish. Since 1997, he has been a Graduate Student Research Assistant at the University of Michigan at Ann Arbor. His research interests are computational electromagnetics, antennas, microwave circuits and systems (MMDS), etc.

Mr. Filipovic received the Nikola Tesla Award from the Serbian Secretary of Science for his diploma thesis.